

Rendezvous Maneuvers of Multiple Spacecraft Using Differential Drag Under J_2 Perturbation

R. Bevilacqua* and M. Romano†

Naval Postgraduate School, Monterey, California 93943

DOI: 10.2514/1.36362

In this work, the residual atmospheric drag is exploited to perform rendezvous maneuvers among multiple spacecraft in low Earth orbits. These maneuvers are required, for instance, for autonomous on-orbit assembly. By varying the level of aerodynamic drag of each spacecraft, relative differential accelerations are generated among the spacecraft of the group and therefore their relative orbits are controlled. Each of the spacecraft is assumed to include a drag plate, which can be actively opened or closed, to vary the atmospheric drag. The recently developed Schweighart–Sedwick model is used to describe the relative dynamics of different spacecraft with respect to a circular orbit with the inclusion of J_2 effects. Furthermore, the natural relative dynamics of each chaser with respect to the target is decoupled into a secular motion and a periodic oscillation. In particular, the following two-phase control method is proposed. First, the secular motion of each chaser is controlled via differential drag in order for the spacecraft to sequentially move from an arbitrary initial condition to a closed stable relative orbit around the target spacecraft. After the relative orbit stabilization, a relative eccentricity control is applied to each spacecraft to zero-out the semi-axis of the relative orbit around the target and to achieve the rendezvous condition. The control algorithm considers mutual constraints among the values of differential drag that the different spacecraft can experience. Potential collisions are avoided by changing the maneuvering initial time. The main advantage of the proposed technique is that it enables a fleet of spacecraft to rendezvous without propellant expenditure. Furthermore, no numerical optimization is needed, because the control policy is based on closed-form analytical solutions. The proposed technique was validated via numerical simulations.

Nomenclature

A = constant coefficient in the state matrix for the transformed state vector
 a = magnitude of differential drag
 a_{ISS} = International Space Station orbit's semimajor axis
 a_{orb} = orbit semimajor axis

B = constant coefficient in state matrix for the transformed state vector
 C_D = drag coefficient
 c = coefficient in Schweighart–Sedwick equations
 d = nonlinear function of Δt^* for computing rendezvous maneuver time duration
 d_c = tolerance distance for collision avoidance



Dr. Riccardo Bevilacqua is an Associate Fellow of the U.S. National Research Council in Mechanical and Astronautical Engineering Department of the Naval Postgraduate School, Monterey, California. He manages the Spacecraft Robotics Laboratory. Dr. Bevilacqua's main research interests are in the dynamics and control of multiple autonomous spacecraft and robotic systems. He received his M.S. in aerospace engineering in 2002 and his Ph.D. in applied mathematics in 2007, both from the University of Rome "La Sapienza," Rome, Italy. He was a Project Engineer at the Grupo Mecanica del Vuelo, Madrid, Spain, during 2003 and a Principal Investigator of the European Space Agency's Ariadna Research Project in 2003. Dr. Bevilacqua is a Member of AIAA.



Dr. Marcello Romano is an Assistant Professor of astronautics in the Mechanical and Astronautical Engineering Department and a member of the Space Systems Academic Group at the Naval Postgraduate School, Monterey, California. He is the Principal Investigator and Project Manager of the Spacecraft Robotics Laboratory and the Small Satellites Dynamics and Control Laboratory. Dr. Romano's main research interests are in the dynamics and control of autonomous spacecraft and robots. He received his M.S. in aerospace engineering in 1997 and his Ph.D. in astronautical engineering in 2001, both from Politecnico di Milano, Milano, Italy. He is the recipient of the 2006 Menneken Annual Faculty Award for Excellence in Scientific Research, awarded by the Naval Postgraduate School Foundation. He was Associate Fellow of the U.S. National Research Council between 2001 and 2003. Dr. Romano is Vice-Chairman of the AIAA Space Automation and Robotics Technical Committee, a Member of the AIAA Guidance Navigation and Control Technical Committee, and a Member of the Space Robotics Technical Committee of the Institute of Electrical and Electronics Engineers. Dr. Romano is a Senior Member of AIAA.

Received 26 December 2007; revision received 17 May 2008; accepted for publication 19 May 2008. This material is declared a work of the U.S. Government and is not subject to copyright protection in the United States. Copies of this paper may be made for personal or internal use, on condition that the copier pay the \$10.00 per-copy fee to the Copyright Clearance Center, Inc., 222 Rosewood Drive, Danvers, MA 01923; include the code 0731-5090/08 \$10.00 in correspondence with the CCC.

*Research Associate, Department of Mechanical and Astronautical Engineering, Code AA/RB, 699 Dyer Road; rbevilac@nps.edu. Member AIAA.

†Assistant Professor, Department of Mechanical and Astronautical Engineering and Space Systems Academic Group, Code MAE/MR, 700 Dyer Road; mromano@nps.edu. Senior Member AIAA.

E	= spacecraft relative mechanical energy with respect to the target (per unit mass)
e	= time-varying eccentricity of the harmonic-oscillator motion
e_{ISS}	= International Space Station orbit's eccentricity
e_0	= time-varying eccentricity of the harmonic-oscillator motion before rendezvous
h	= target altitude above the Earth's surface
i_{ref}	= reference local-vertical/local-horizontal orbit inclination
i_{ISS}	= International Space Station orbit's inclination
J_2	= second-order harmonic of Earth's gravitational potential field (Earth flattening) ($108,263 \times 10^{-8}$)
k	= coefficient in Schweighart–Sedwick equations
l	= coefficient in Schweighart–Sedwick equations (out-of-plane motion)
m	= spacecraft mass
N_S	= number of spacecraft in the fleet
q	= coefficient in Schweighart–Sedwick equations (out-of-plane motion)
R_{\oplus}	= Earth's mean radius (6378.1363 km)
r_{ref}	= reference local-vertical/local-horizontal orbit radius
S	= spacecraft wind cross-sectional area
s	= coefficient in Schweighart–Sedwick equations
T	= orbital period
t	= time
t_{s_i}	= i th sign switching instant for differential drag
u, U	= control variable
V	= spacecraft velocity vector with respect to Earth's atmosphere
\hat{V}	= spacecraft velocity unit vector with respect to Earth's atmosphere
x, y, z	= position coordinates of the target in local-vertical/local-horizontal
$\dot{x}, \dot{y}, \dot{z}$	= velocity components of the target in local-vertical/local-horizontal
z	= transformed spacecraft relative state vector, $[z_1 \ z_2 \ z_3 \ z_4]^T$
z'	= intermediate transformed spacecraft relative state vector, $[z'_1 \ z'_2 \ z'_3 \ z'_4]^T$
ΔE	= energy deadband
Δt_s	= sample time interval
Δt_w	= waiting time interval before the controlled phase in rendezvous maneuver
Δt^*	= unknown time duration for the controlled rendezvous phases
$\Delta x, \Delta y, \Delta z$	= mutual position coordinates of two spacecraft in local-vertical/local-horizontal
$\Delta \dot{x}, \Delta \dot{y}, \Delta \dot{z}$	= mutual velocity components of two spacecraft in local-vertical/local-horizontal
ϕ	= phase of the forcing term in out-of-plane motion in Schweighart–Sedwick equations
ν	= Earth's gravitational constant ($398600.4418 \text{ km}^3 \text{ s}^{-2}$)
ν_{ISS}	= International Space Station orbit's generic true anomaly (at initial time)
ρ	= atmospheric density
Ω_{ISS}	= International Space Station orbit's right ascension of ascending node (raan)
ω	= target's circular-orbit angular velocity
ω_{ISS}	= International Space Station orbit's argument of perigee

Subscripts

j	= component along the j direction in local-vertical/local-horizontal ($j = x, y, z$)
0	= initial conditions

I. Introduction

THIS paper introduces a novel control method for autonomous orbit stabilization and rendezvous of a group of multiple spacecraft by using the differential aerodynamic drag. The proposed method can be used, for instance, for an on-orbit assembly mission. By varying the level of aerodynamic drag of each spacecraft, relative differential accelerations are generated among the spacecraft of the group and therefore their relative orbits are controlled. The first obvious advantage of this technique is the propellant savings with respect to standard control by thrusters. A further advantage is avoiding thrusters' plume impingement when spacecraft are close.

The use of aerodynamic drag to control low-Earth-orbiting spacecraft has been studied in [1,2] for the orbit control of a single spacecraft and in [3–6] for the formation-keeping and rendezvous of two spacecraft.

Most of the authors who focus on low-thrust proximity maneuvers (see, for instance, [1–9]) use the classic Hill–Clohessy–Wiltshire linear model [10]. However, when the maneuver lasts for several orbits, a different representation of the relative dynamics is desired to take into account differential effects on the spacecraft motion due to the Earth's flattening (J_2 perturbation).

The main contributions of the present work, which are original to the best of our knowledge, are as follows:

1) We have significantly improved the method proposed by Leonard et al. [5,6] for the single-chaser/single-target rendezvous with no J_2 effect, which we used as a starting point for our study. In particular,

a) We have eliminated the problem of having a residual distance between the chaser and the target at the end of the maneuver.

b) We have eliminated the need of using a numerical optimization routine, because the maneuver is based on an analytical expression.

2) We have developed a control policy based on aerodynamic drag for the rendezvous of a set of more than two spacecraft.

3) We have considered the presence of the J_2 perturbation in the dynamic model used by the controller. In particular, we used the model developed by Schweighart and Sedwick [11]. Nevertheless, the proposed approach can also be used with the simpler Hill–Clohessy–Wiltshire model.

The main difficulty when dealing with more than two spacecraft is to respect the existing constraints among the values of differential drag that the spacecraft can experience. In fact, at a given time, some chaser spacecraft may need a drag force higher than the target's, whereas other chaser spacecraft may need a drag force equal to or lower than the target's. These conflicts are here resolved through the introduction of a sequential logic based on the value of the relative mechanical energy of each chaser spacecraft with respect to the target.

The proposed control approach consists of the following two successive phases:

1) First, all of the chaser spacecraft (of arbitrary number N_S) are driven to closed relative orbits with respect to the target spacecraft. This stabilization is performed by simultaneously controlling the differential aerodynamic drag.

2) Second, additional closing maneuvers are performed by each spacecraft, one at a time, in order to have all of the spacecraft converging to the target.

The paper is organized as it follows: Section II presents the dynamic model. Section III introduces the control algorithms. Section IV reports the results of the numerical simulations. Section V concludes the paper.

II. Model of Relative Spacecraft Dynamics and Actively Controlled Differential Drag

The linearized dynamic model of a spacecraft moving with respect to a circular orbit, including the J_2 effects, as introduced by Schweighart and Sedwick in [11], is

$$\begin{cases} \ddot{x} = 2(\omega c)\dot{y} + (5c^2 - 2)\omega^2 x - 3\omega^2 J_2 (R_\oplus^2 / r_{\text{ref}}) \\ \left\{ \frac{1}{2} - [3\sin^2 i_{\text{ref}} \sin^2(kt)/2] - [(1 + 3 \cos 2i_{\text{ref}})/8] \right\} + U_x \\ \ddot{y} = -2(\omega c)\dot{x} - 3\omega^2 J_2 (R_\oplus^2 / r_{\text{ref}}) \sin^2 i_{\text{ref}} \sin(kt) \cos(kt) + U_y \\ \ddot{z} = -q^2 z + 2lq \cos(qt + \phi) + U_z \end{cases} \quad (1)$$

$$k = \omega c + \frac{3\omega J_2 R_\oplus^2}{2i_{\text{ref}}^2} \cos^2 i_{\text{ref}}$$

where the coordinate system is thus defined: the x axis points from the center of the Earth to the origin of the system (which moves along a circular orbit), the y axis is along the orbital track, and the z axis completes a right-hand Cartesian coordinate system. The angular velocity of the coordinate system with respect to the inertial frame is [11]

$$\omega c, \quad c = \sqrt{1 + \frac{3J_2 R_\oplus^2}{8r_{\text{ref}}^2} (1 + 3 \cos 2i_{\text{ref}})} \quad (2)$$

In the present paper, one of the spacecraft in a fleet of multiple spacecraft is arbitrarily chosen as the target and all of the other spacecraft need to maneuver to reach it. Therefore, of particular interest for our purposes are the following equations describing the relative dynamics between a generic spacecraft of the fleet and the target [11]:

$$\begin{cases} \Delta \ddot{x} = 2(\omega c)\Delta \dot{y} + (5c^2 - 2)\omega^2 \Delta x + u_x \\ \Delta \ddot{y} = -2(\omega c)\Delta \dot{x} + u_y \\ \Delta \ddot{z} = -q^2 \Delta z + 2lq \cos(qt + \phi) + u_z \end{cases} \quad (3)$$

where $[u_x \ u_y \ u_z]$ indicate the components of the relative acceleration between the two spacecraft due to a control action.

Equations (1) and (3) reduce to the Hill–Clohessy–Wiltshire equations if the J_2 effect is not considered [i.e., when $c = 1$ and $l = q = 0$ (see [11])]. Therefore, all of the developments of the

present work remain valid if the simpler Hill–Clohessy–Wiltshire model is used.

The acceleration on a spacecraft due to the atmospheric drag can be expressed as [5,6]

$$\mathbf{a} = \left(-\frac{\rho S C_D}{2m} v^2 \right) \hat{\mathbf{v}} \quad (4)$$

For spacecraft able to change their wind cross-sectional surface area S , this acceleration can be considered as a control vector, with the only nonzero component u_y in Eq. (3). The simplifying assumption of controlling only along y can be found in several works, not only limited to drag control techniques [7,12,13]. A controlled variation of the wind cross surface S can be achieved, for instance, by changing the attitude of the spacecraft or, as considered in this paper, by opening and closing a drag plate.

We consider the following modeling assumptions for our study (see Fig. 1):

1) The angle of attack of the drag plate of each spacecraft can be either 0 or 90 deg, thus generating either a minimum or a maximum drag force (off–on), with no intermediate values considered possible.

2) Attitude dynamics is not considered. Attitude is assumed to be stabilized.

3) All of the spacecraft in the fleet have the same drag coefficient and mass.

4) The air density is constant for all of the spacecraft and equal to that of the target's altitude at the initial time t_0 .

5) The problem is confined to the x – y plane. Therefore, for each chaser, the state vector is $[\Delta x \ \Delta y \ \Delta \dot{x} \ \Delta \dot{y}]^T$ and the final condition is $[\Delta x \ \Delta y \ \Delta \dot{x} \ \Delta \dot{y}]^T = [0 \ 0 \ 0 \ 0]^T$. The control of the dynamics along the z axis, which is oscillatory and independent from the one on the x – y plane, is considered to be beyond of the scope of the present paper.

6) The target orbital rate ω is constant during the maneuver.

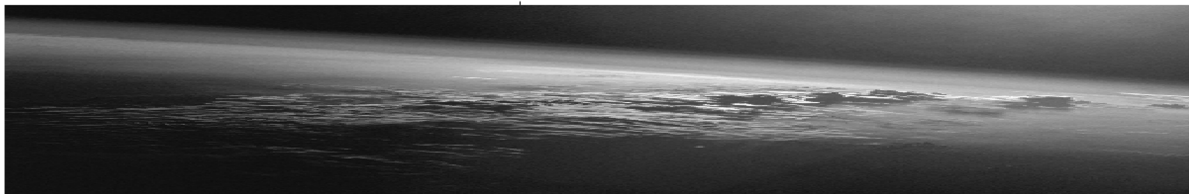
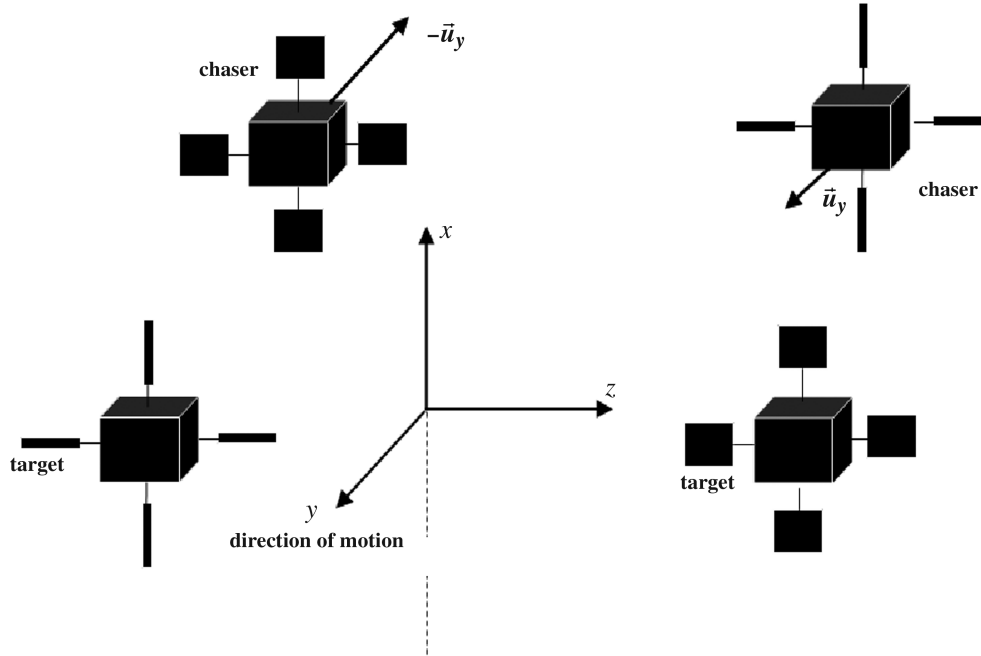


Fig. 1 Conceptual explanation of the differential drag control. If the chaser opens its drag plates it causes a relative negative acceleration of the chaser with respect to the target; if the target opens its drag plates it causes a relative positive acceleration of the chaser with respect to the target.

This section summarizes the results of [14], in which we applied a state vector transformation to Eq. (3) to separate the mean secular motion from the oscillatory part. The generic chaser's state vector $[\Delta x \ \Delta y \ \Delta \dot{x} \ \Delta \dot{y}]^T$ of the Schweighart–Sedwick equations is transformed into a new intermediate state vector $[z'_1 \ z'_2 \ z'_3 \ z'_4]^T$ by

$$\begin{bmatrix} z'_1 \\ z'_2 \\ z'_3 \\ z'_4 \end{bmatrix} = \begin{bmatrix} 0 & 1 & -\frac{A}{A^2-B} & 0 \\ -\frac{BA}{A^2-B} & 0 & 0 & -\frac{B}{A^2-B} \\ 0 & 0 & -\frac{A^2}{2(A^2-B)^{3/2}} & 0 \\ -\frac{A^2B}{2(A^2-B)^{3/2}} & 0 & 0 & -\frac{A^3}{2(A^2-B)^{3/2}} \end{bmatrix} \begin{bmatrix} \Delta x \\ \Delta y \\ \Delta \dot{x} \\ \Delta \dot{y} \end{bmatrix} \quad (5a)$$

$A = 2(\omega c) \quad B = (5c^2 - 2)\omega^2$

where $A^2 - B$ is an always-positive constant.

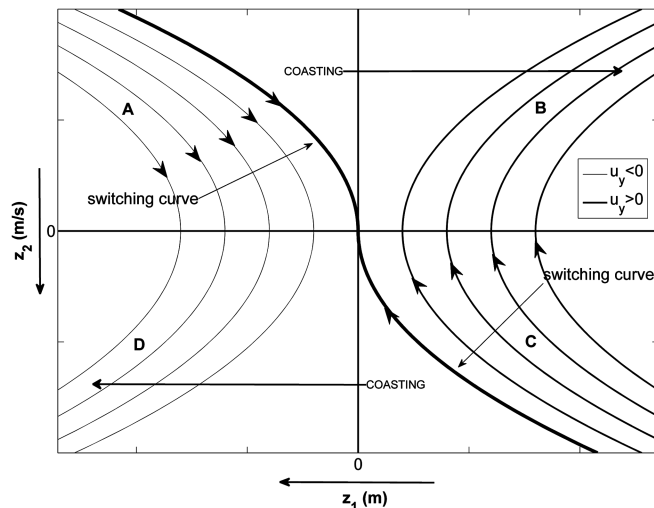
Equation (5b) reports the inverse transformation of Eq. (5a):

$$\begin{bmatrix} \Delta x \\ \Delta y \\ \Delta \dot{x} \\ \Delta \dot{y} \end{bmatrix} = \begin{bmatrix} 0 & -\frac{A}{B} & 0 & -\frac{2\sqrt{A^2-B}}{A^2} \\ 1 & 0 & \frac{2\sqrt{A^2-B}}{A} & 0 \\ 0 & 0 & -\frac{2\sqrt{(A^2-B)^3}}{A^2} & 0 \\ 0 & 1 & 0 & \frac{2\sqrt{A^2-B}}{A} \end{bmatrix} \begin{bmatrix} z'_1 \\ z'_2 \\ z'_3 \\ z'_4 \end{bmatrix} \quad (5b)$$

By expressing $[\Delta x \ \Delta y \ \Delta \dot{x} \ \Delta \dot{y}]^T$ as a function of $[z'_1 \ z'_2 \ z'_3 \ z'_4]^T$ [Eq. (5b)], substituting $[\Delta x \ \Delta y \ \Delta \dot{x} \ \Delta \dot{y}]^T$ into Eq. (3), and considering only a control component along y , it follows that

$$\begin{bmatrix} \dot{z}'_1 \\ \dot{z}'_2 \\ \dot{z}'_3 \\ \dot{z}'_4 \end{bmatrix} = \begin{bmatrix} 0 & 1 & 0 & 0 \\ 0 & 0 & 0 & 0 \\ 0 & 0 & 0 & 1 \\ 0 & 0 & -(A^2 - B) & 0 \end{bmatrix} \begin{bmatrix} z'_1 \\ z'_2 \\ z'_3 \\ z'_4 \end{bmatrix} + \begin{bmatrix} 0 \\ -\frac{B}{A^2-B} \\ 0 \\ \frac{A^3}{2(A^2-B)^{3/2}} \end{bmatrix} u_y \quad (6)$$

which is the combination of a double integrator and a harmonic oscillator. Equation (6) has the following closed-form solution for constant control acceleration u_y :



a) Qualitative shape of the curves in z_1-z_2

$$\begin{aligned} z'_1 &= -\frac{B}{A^2-B} u_y \frac{t^2}{2} + z'_{2_0} t + z'_{1_0} & z'_2 &= -\frac{B}{A^2-B} u_y t + z'_{2_0} \\ z'_3 &= \left(z'_{3_0} - \frac{A^3 u_y}{2(A^2-B)^{5/2}} \right) \cos[(\sqrt{A^2-B})t] \\ &\quad + \frac{z'_{4_0}}{\sqrt{A^2-B}} \sin[(\sqrt{A^2-B})t] + \frac{A^3 u_y}{2(A^2-B)^{5/2}} \\ z'_4 &= z'_{4_0} \cos[(\sqrt{A^2-B})t] \\ &\quad - \sqrt{A^2-B} \left(z'_{3_0} - \frac{A^3 u_y}{2(A^2-B)^{5/2}} \right) \sin[(\sqrt{A^2-B})t] \end{aligned} \quad (7a)$$

For notational convenience, we will use the following modified final transformed state vector in the rest of the paper:

$$z_1 = z'_1 \quad z_2 = z'_2 \quad z_3 = z'_3 \quad z_4 = \frac{z'_4}{\sqrt{A^2-B}} \quad (7b)$$

By eliminating the time variable from the first two equations of Eq. (7), it follows that the motion in the z_1-z_2 plane occurs along parabolas, with positive or negative concavity depending on the sign of the differential drag (see Fig. 2a).

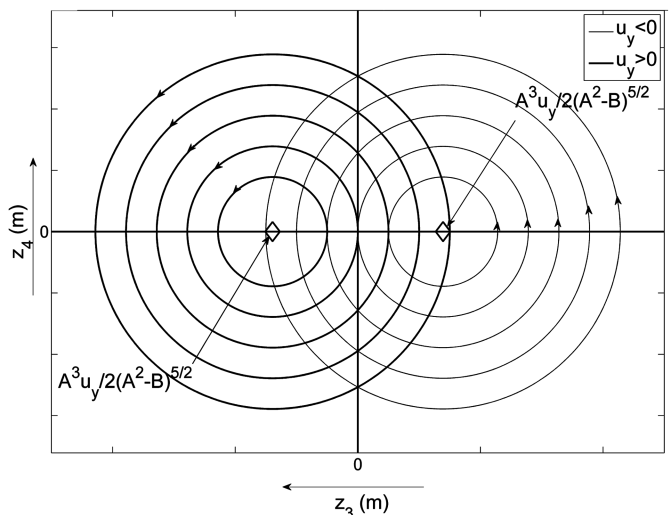
Furthermore, by eliminating the time variable from the last two equations of Eq. (7), it follows that the motion in the z_3-z_4 plane occurs along circles centered at the points

$$\left[\frac{A^3 u_y}{2(A^2-B)^{5/2}} \quad 0 \right]$$

with either $u_y > 0$ or $u_y < 0$ (see Fig. 2b).

As can be easily demonstrated from Eq. (7), the uncontrolled trajectories (coasting) in the z_1-z_2 plane correspond to horizontal straight lines traveled, with a direction dependent on the sign of the initial z_2 , and in the z_3-z_4 plane, they correspond to circles centered at the origin, with a radius equal to the initial distance from the origin and traveled in the counterclockwise direction. All of the state variables (in both the phase planes) need to be controlled to move toward the desired final rendezvous condition of zero relative position and velocity.

The bold curves in Fig. 2a are the switching curves, taking the average position of the chaser with respect to the target directly to the origin without additional need of switching the sign. The distance from the origin of a point on the curves in Fig. 2b is given, at any time, by



b) Qualitative shape of the curves in z_3-z_4

Fig. 2 Qualitative shape of the curves representing the relative motion of a chaser with respect to the target in the phase planes. The axis orientation has been chosen consistent with [5].

$$e = \sqrt{z_3^2 + z_4^2} \quad (8)$$

This quantity will be called the eccentricity of the harmonic motion [5].

III. Multispacecraft Control Algorithm

The aim of the proposed maneuver, thought to be in preparation of an eventual assembly, is to drive the state of each chaser to the origin of both phase planes in Fig. 2. The maneuver is conducted in the following two successive phases:

- 1) In the stabilization phase, each chaser spacecraft is driven to a stable periodic orbit around the target.
- 2) In the rendezvous phase, each chaser spacecraft converges to the target.

A. Two-Spacecraft Case (One Chaser and One Target)

Let us consider first, for explanation purposes, to have only two spacecraft in the fleet (one chaser and one target). A negative relative acceleration along the y axis of the chaser with respect to the target, due to drag appearing if the chaser is opening the plate but the target is not. Conversely, a positive acceleration of the chaser with respect to the target appears if the target is opening the plate but the chaser is not. No relative acceleration appears when both vehicles have their plates either open or closed.

1. Phase 1: Relative Orbit Stabilization

The conditions to be satisfied to have closed relative orbits, as can be demonstrated from Eq. (3), are [11]

$$\begin{aligned} \Delta \dot{x} &= \frac{\omega \Delta y (1-s)}{2 \sqrt{1+s}} & \Delta \dot{y} &= -2\omega \Delta x \sqrt{1+s} \\ s &= \frac{3J_2 R_{\oplus}^2}{8R^2} (1 + 3 \cos 2i_{\text{ref}}) \end{aligned} \quad (9)$$

A particular case of this condition is when $\Delta x = \Delta \dot{x} = 0$ (i.e., for a leader-follower configuration, which is a particular admissible case of stable relative orbit). Equation (9) corresponds to $z_1 = z_2 = 0$, as can be demonstrated by equating to zero the first two equations of Eq. (5).

Notably, if the differential drag has the opposite sign of z_4 , the value of e reduces with time. In fact, by taking the derivative with respect to time of Eq. (8) and by considering Eq. (7), it follows that

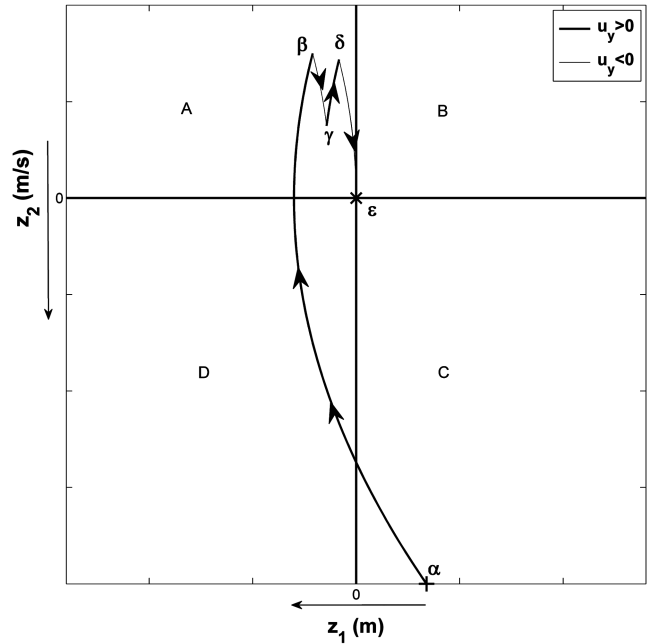
$$\frac{d(e^2)}{dt} = 2\omega \frac{A^3 u_y}{2(A^2 - B)^{5/2}} z_4 \quad (10)$$

The control sequence has to take into account the conditions related to each of the two phase planes at the same time. In fact, if we consider only the double-integrator portion of the dynamics (see Fig. 2a), by switching the sign of the relative acceleration just once, at the point at which one of the two switching curves is reached, the spacecraft state variables (z_1, z_2) would go to the origin in a minimum time [15]. But this control procedure could result in a high residual eccentricity e [see Fig. 2b and Eqs. (5) and (6)].

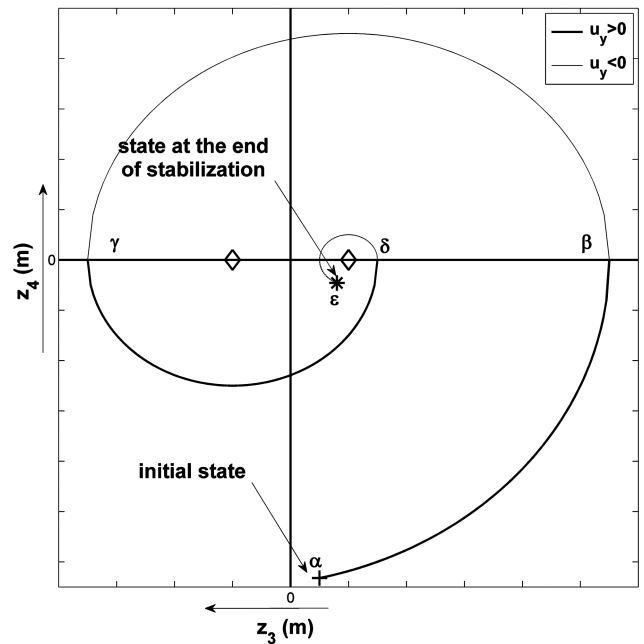
On the other hand, if we consider only the harmonic-oscillator portion of the dynamics (see Fig. 2b), by suitably switching the sign of the relative acceleration, as dictated by the optimal control theory, the spacecraft state variables (z_3, z_4) go to the origin in a minimum time (see [15]). But this control procedure would result, in general, in a residual drift of the chaser with respect to the target.

Therefore, to simultaneously control the four state variables (z_1, z_2, z_3, z_4) on the two phase planes of Fig. 2, the following algorithmic steps are applied (see also Fig. 3):

1) If, at the beginning of the maneuver, the point (z_1, z_2) is either in the A quadrant of Fig. 2a at the left-hand side of the switching curve or in the C quadrant at the right-hand side of the switching curve, then go directly to step 2. Conversely, if at the beginning of the maneuver the point (z_1, z_2) is either on the right-hand side of the control



a) Stabilization trajectory in the z_1 - z_2 plane



b) Stabilization trajectory in the z_3 - z_4 plane

Fig. 3 Qualitative example of relative orbit stabilization maneuver in the phase planes. The + on the trajectory indicates the initial state, and the * indicates the final condition at the exit of the stabilization algorithm. Equal Greek letters in the two figures indicate simultaneous events.

switching curve for $z_2 < 0$ or on the left-hand side of the switching curve for $z_2 > 0$ (see Fig. 2a), then either a negative or a positive relative acceleration is applied, respectively, until either the C quadrant or the A quadrant is reached. Then go to step 2.

2) Either a positive relative acceleration is applied if the point (z_1, z_2) is in the A quadrant of Fig. 2a, or a negative acceleration if the point is in the C quadrant, until any one of the following three conditions is met:

- a) The sign of the variable z_4 switches. Then go to step 3.
- b) The condition $e < (A^3 u_y / (A^2 - B)^{5/2})$ becomes true. Then go to step 4.
- c) One of the two switching curves of Fig. 2a is reached. Then go to step 5.

3) The sign of the relative acceleration is switched and is then kept constant until any one of the three conditions considered during step 2 is met again. Then the indications reported after the met conditions are followed.

4) Either a positive relative acceleration is applied if the point (z_1, z_2) is in the A quadrant of Fig. 2a, or a negative acceleration is applied if the point is in the C quadrant, until one of the two switching curves of Fig. 2a is reached. Go to step 5.

5) The sign of the relative acceleration is switched for the last time. When the point (z_1, z_2) reaches the origin, the sign of the relative acceleration is switched off, and the stabilization algorithm stops.

The quadrants A and C of Fig. 2a are called sawtooth zones, due to the shape of the curve resulting from the application of the preceding algorithm on the z_1 - z_2 phase plane (see Fig. 3).

Notably, at any time during the iterative repetition of the steps 3 and 2a, the future sign switches of z_4 are given, based on the current values of (z_3, z_4) , by

$$t_{s_k} = \frac{1}{\sqrt{A^2 - B}} \left[\tan^{-1} \left(z_4 / \left(z_3 - \frac{A^3 u_y}{2(A^2 - B)^{5/2}} \right) \right) + k\pi \right] \quad (11)$$

as can be demonstrated by equating to zero the last equation of Eq. (7).

Furthermore, the conditional step 2b is based on the fact that there is no benefit, as far as eccentricity reduction, in switching the control sign according to the sign of z_4 (every half orbital period) when $e < (A^3 u_y / (A^2 - B)^{5/2})$.

2. Phase 2: Rendezvous to the Target

This section introduces a new method, exploiting the differential drag, to drive to zero the relative state vector of a single chaser spacecraft with respect to the target (i.e., to reach the condition $z_1 = z_2 = z_3 = z_4 = 0$) once the condition of stable relative orbit ($z_1 = z_2 = 0$) has been reached, as described in the previous section.

In particular, the trajectory in the z_1 - z_2 plane during the rendezvous maneuver is assumed to be one element of the set S_{12} of infinite trajectories that start from the origin of the phase plane and

In detail, the following steps were followed to obtain the analytic solution for the value of Δt^* (see also Fig. 4):

1) From Eq. (7), considering the desired rendezvous ($z_3 = z_4 = 0$) as the initial condition, the analytic symbolic expression is obtained for the state reached in the z_3 - z_4 phase plane by applying either the maximum or the minimum acceleration for an arbitrary backward time interval $-\Delta t^*$. The decision of which sign of acceleration to use will become clear later. Let us use the expression $[^+z_3(-\Delta t^*) \ ^+z_4(-\Delta t^*)]$ to indicate the state reached with maximum acceleration and the expression $[^-z_3(-\Delta t^*) \ ^-z_4(-\Delta t^*)]$ to indicate the state reached with minimum acceleration. Furthermore, for nomenclature convenience, let us use the expression $[^\pm z_3(-\Delta t^*) \ ^\pm z_4(-\Delta t^*)]$ to indicate both cases.

2) From Eq. (7), considering the initial condition to be the one achieved at the end of step 1, the analytic symbolic expression is obtained for the state reached by applying the extremal acceleration of opposite sign with respect to that of step 1 for a backward time interval $-2\Delta t^*$. The two possible reached states are indicated by the expression $[^\pm z_3(-3\Delta t^*) \ ^\pm z_4(-3\Delta t^*)]$.

3) From Eq. (7), considering the initial condition to be the one achieved at the end of step 2, the analytic symbolic expression is obtained for the state reached by applying the extremal acceleration of same sign with respect to that of step 1 for a backward time interval $-\Delta t^*$. The two possible reached states are indicated by the expression $[^\pm z_3(-4\Delta t^*) \ ^\pm z_4(-4\Delta t^*)]$.

4) The following analytic symbolic expression is found for the distance between the state obtained in the z_3 - z_4 plane at the end of step 3 and the circle of radius e_0 , which is the orbit reached at the end of the stabilization phase:

$$^\pm d(\Delta t^*) = e_0 - \sqrt{(\pm z_3(-4\Delta t^*))^2 + (\pm z_4(-4\Delta t^*))^2} \quad (12)$$

5) By equating to zero the expression in Eq. (12), the following equation in the unknown Δt^* is found, which is independent from the particular acceleration sign sequence used:

$$^+d(\Delta t^*) = ^-d(\Delta t^*) = e_0 + K \sqrt{(-5 + 4 \cos(f\Delta t^*) - 4 \cos(3f\Delta t^*) + \cos(4f\Delta t^*) + 4 \cos(2f\Delta t^*))} = 0$$

$$f = \sqrt{A^2 - B} \quad K = -\frac{\sqrt{2} A^3 |u_y|}{2 f^5} i \quad (13)$$

are composed of the following three controlled phases (see also Fig. 4a): 1) a maximum (or minimum) acceleration phase of arbitrary time duration Δt^* , 2) a minimum (or maximum) acceleration phase of time duration $2\Delta t^*$, and 3) a maximum (or minimum) acceleration phase of time duration Δt^* .

These trajectories are closed and symmetric with respect to the z_1 axis.

Furthermore, the trajectory in the z_3 - z_4 plane during the same maneuver is assumed to be one element of the set S_{34} of ∞^2 trajectories that start from the state at the end of the relative orbit stabilization and are composed of 1) an initial coasting phase of arbitrary duration Δt_w and 2) a sequence of three controlled phases of total duration $4\Delta t^*$, corresponding to the phases of the trajectories on the z_1 - z_2 plane that are part of the set S_{12} .

The specific values of Δt^* and Δt_w and of the acceleration sign sequence are chosen to be those that identify, among the elements of the set S_{34} , the shortest (in time) trajectory that connects the state at the end of the stabilization phase ($[\bar{z}_3 \ \bar{z}_4]$) to the desired final rendezvous condition ($z_3 = z_4 = 0$).

where i is the imaginary unit. Four solutions of Eq. (13) exist, of which two are real and two are complex conjugates. The smallest one between the two real solutions is chosen as the required Δt^* . This solution is

$$\Delta t^* = \frac{1}{f} \cos^{-1} \left(\frac{1}{2} + \frac{1}{12} \sqrt{36 + \frac{6\sqrt[3]{H}}{K} - \frac{36e_0^2}{K\sqrt[3]{H}}} \right) - \frac{\sqrt{6}}{12} \sqrt{12 - \frac{\sqrt[3]{H}}{K} + \frac{6e_0^2}{K\sqrt[3]{H}} - \left(72 / \sqrt{36 + \frac{6\sqrt[3]{H}}{K} - \frac{36e_0^2}{K\sqrt[3]{H}}} \right)}$$

$$H = -54Ke_0^2 + 6\sqrt{3}e_0^2 \sqrt{2e_0^2 + 27K^2} \quad (14)$$

In summary, this Δt^* guarantees reaching the rendezvous condition by following a maneuver consisting of three bang-bang controlled periods (of respective durations Δt^* , $2\Delta t^*$, and Δt^*), starting from a state $[^\pm z_3(-4\Delta t^*) \ ^\pm z_4(-4\Delta t^*)]$ along the stable orbit reached at the end of the stabilization phase.

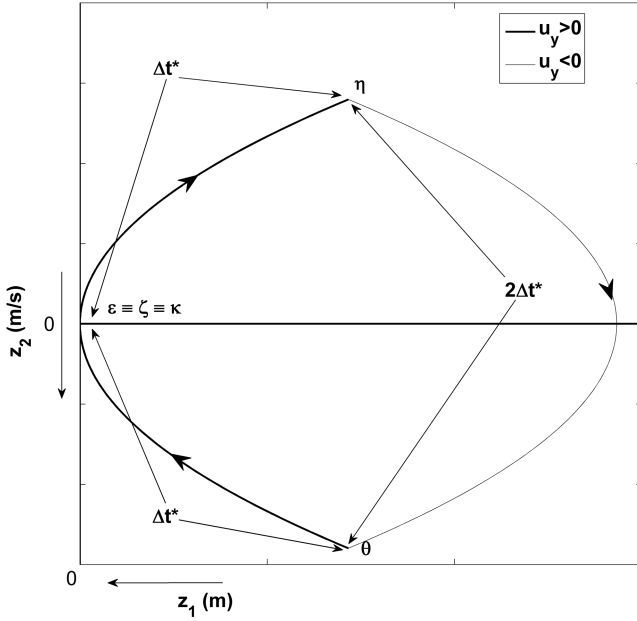
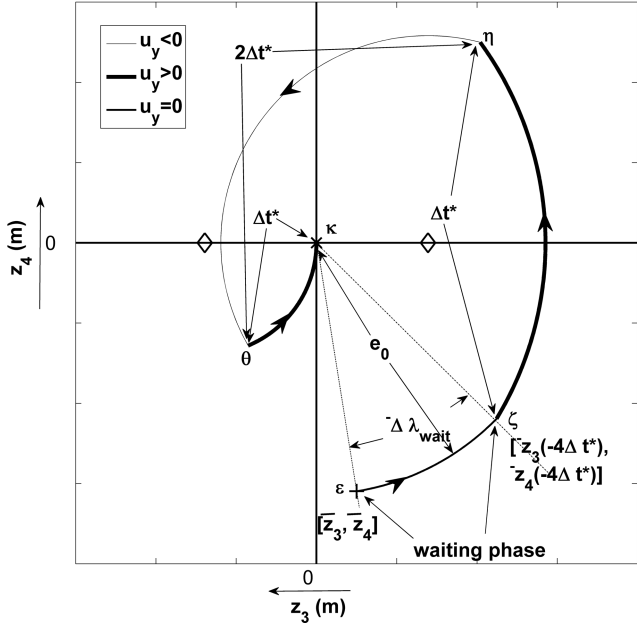
a) Rendezvous trajectory in the z_1 - z_2 planeb) Rendezvous trajectory in the z_3 - z_4 plane

Fig. 4 Qualitative example of rendezvous maneuver in the phase planes. The + indicates the initial state, and the x indicates the final condition.

The value of the duration Δt_w of the initial coasting along that stable orbit is straightforwardly found by solving the following equation:

$$\begin{aligned} \Delta t_w &= \min \left(\left| \frac{\pm \Delta \lambda_{\text{wait}}}{f} \right| \right) \\ &= \frac{1}{f} \min \left(\left| \tan^{-1} \left(\frac{\pm z_3(-4\Delta t^*)}{\pm z_4(-4\Delta t^*)} \right) - \tan^{-1} \left(\frac{z_3}{z_4} \right) \right| \right) \end{aligned} \quad (15)$$

Finally, the acceleration sign sequence is chosen, among the two possible sequences, which corresponds to the duration Δt_w .

The solution proposed in this section presents the following significant advantages with respect to that proposed in [5]:

1) The rendezvous control policy developed here drives the whole state vector of the chaser to zero, whereas the procedure in [5] always results in a final residual distance of the chaser from the target.

2) It is an analytical solution on a single variable, whereas a numerical optimization solution is required in [5], in which two different time durations have to be computed.

3) The time required for the maneuver is much lower, as it is shown in the following numerical simulations.

B. Multiple-Spacecraft Case ($N_s - 1$ Chasers, One Target, with $N_s > 2$)

1. Phase 1: Relative Orbit Stabilization of Multiple Spacecraft

A centralized heuristic control logic is here proposed to stabilize the orbits of multiple chaser spacecraft about the target by exploiting the differential drag. When multiple chaser spacecraft are involved, the problem becomes more challenging because the achievable levels of differential drag between each chaser and the target are mutually constrained. Consider, as an example, the case when some of the chasers' orbits around the target are already stabilized but others are not. If the stabilization of one of the remaining unstable chasers requires the target to experience maximum drag, the already stabilized chasers have to open their plates as well, for the sake of keeping their relative stabilization.

In particular, the proposed control logic is composed of the following algorithmic steps. These steps are iteratively executed until the desired condition of orbit stabilization is reached for all of the chaser spacecraft (i.e., until it is $z_1 = z_2 = 0$ for each chaser with respect to the target):

1) The required relative acceleration is computed at the beginning of each sample time interval Δt_s for each of the chaser spacecraft that remain to be stabilized around the target. The control algorithm described in Sec. III.A.1 for a single chaser spacecraft is used to compute the required acceleration.

2) If the required relative accelerations computed in step 1 are all in accordance with each other, they are commanded (and generated by synchronously maneuvering the drag plates of all of those chasers). Otherwise, if not all of the required relative accelerations computed in step 1 are in accordance with each other, then the level of relative acceleration applied to all of the chasers that remain to be stabilized around the target is decided based on the following prioritized list of conditions:

a) When one of the not-yet-stabilized chaser spacecraft reaches a switching curve (Fig. 2a), the relative acceleration that brings that spacecraft to a stable orbit (i.e., to the condition $z_1 = z_2 = 0$) is considered as the reference acceleration until the stabilization is achieved (for that single spacecraft). Those chasers requiring an opposite sign acceleration from step 1 experience zero control (coasting); the others will experience the reference acceleration.

b) When one of the not-yet-stabilized chaser spacecraft meets condition 2b of Sec. III.A.1, its desired relative acceleration (according to algorithm in Sec. III.A.1) is considered as the reference acceleration until the stabilization is achieved. Those chasers requiring an opposite sign acceleration from step 1 experience zero control (coasting); the others will experience the reference acceleration. The occurrence of condition 2a would cause an immediate jump to case 2a.

c) When one of the not-yet-stabilized chaser spacecraft crosses the z_1 axis (Fig. 2a) and enters into one of the sawtooth zones, its desired relative acceleration value is considered as the reference acceleration until one of the conditions (2a, 2b, or 2c) of Sec. III.A.1 is verified. Those chasers requiring an opposite sign acceleration from step 1 experience zero control (coasting); the others will experience the reference acceleration.

Table 1 Spacecraft characteristics and atmospheric density

Mass, kg	10
S , m^2	1
C_D	2.2
h , km	350
$\rho_{350 \text{ km}}$, $\text{kg} \cdot \text{m}^{-3}$	6.98×10^{-12} ([16])
$i_{\text{ref}} = i_{\text{ISS}}$, deg	51.595

Table 2 Initial conditions for simulation

	z_{10} , m	z_{20} , m/s	z_{30} , m	z_{40} , m	$[x_0 \ y_0]$, m	$[\dot{x}_0 \ \dot{y}_0]$, m/s
Sat ₁	-609	0.86	128	43.71	[-528.38 - 481]	[0.07 0.92]
Sat ₂	-609	-0.86	128	-43.71	[528.38 - 481]	[0.07 - 0.92]
Sat ₃	-509	-0.69	128	52.45	[379.62 - 381]	[0.07 - 0.64]
Sat ₄	309	-0.52	128	52.45	[279.62 437]	[0.07 - 0.47]
Sat ₅ (target)	0	0	0	0	[0 0]	[0 0]

Table 3 Simulation parameters

Δt_s	10 s
ΔE	Dynamic: half of the current maximum energy
d_c	20 m

d) When none of the three preceding conditions are satisfied, a reference relative acceleration value is computed for all the not-yet-stabilized chasers, which is equal to the acceleration desired by the chaser spacecraft that has the highest relative energy with respect to the target, as determined by

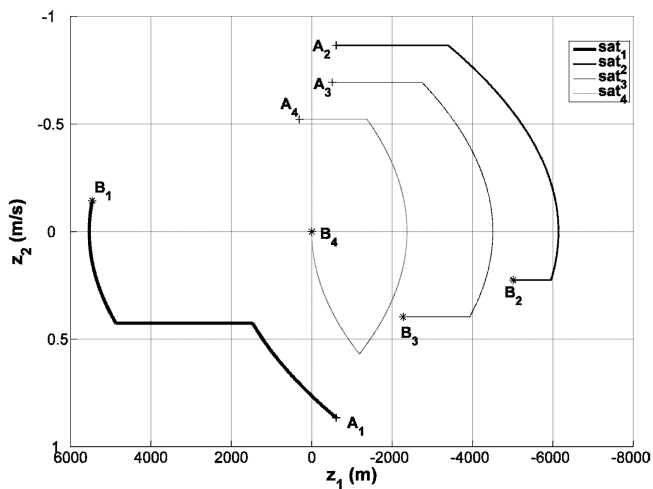
$$\begin{aligned}
 E &= v\sqrt[3]{R|x|} + \dot{x}^2 + \dot{y}^2 \\
 &= v\sqrt[3]{R} \left| -\frac{A^3 z_2 + 2Bz_4}{A^2 B} \right| + \left(\frac{2\sqrt{A^2 - Bz_3}}{A^2} \right)^2 \\
 &\quad + \left(\frac{Az_2 + 2z_4}{A} \right)^2
 \end{aligned} \tag{16}$$

Those chasers requiring an opposite sign acceleration from step 1 experience zero control (coasting); the others will experience the reference acceleration.

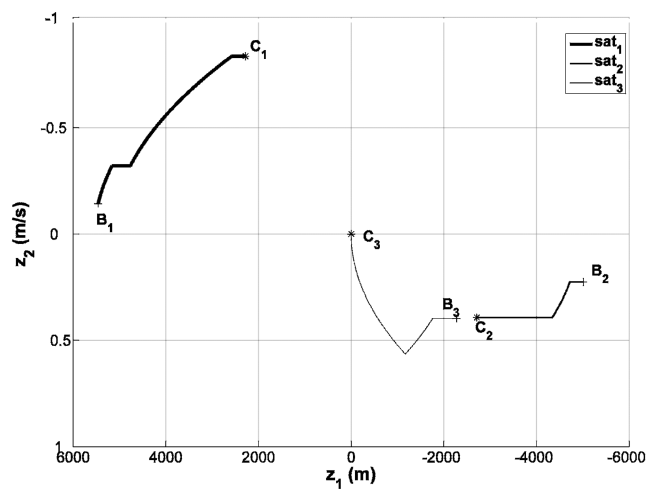
An energy deadband ΔE is used to avoid chattering among different values of acceleration when the energies of different spacecraft become comparable. The occurrence of any of conditions 2a, 2b, or 2c will cause an immediate jump to the corresponding case.

2. Phase 2: Rendezvous of Each Chaser Spacecraft to the Target

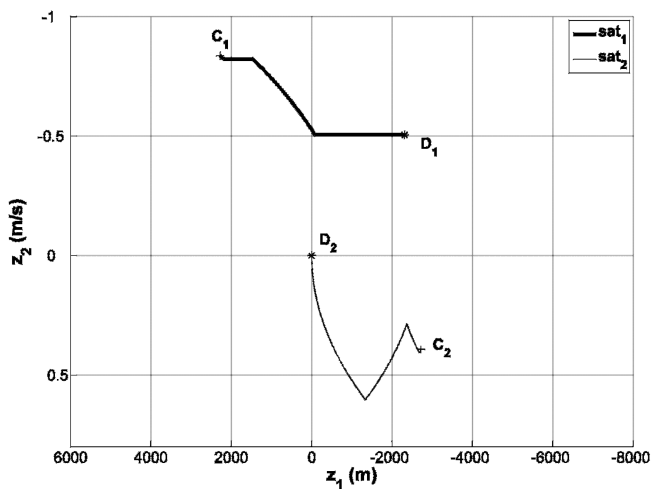
After every chaser spacecraft has been stabilized about the target, the rendezvous with the target of each chaser at a time is sequentially performed by following the algorithm introduced for the two-spacecraft case in Sec. III.A.2. In particular, the chaser to maneuver first is the one that has the smallest relative orbit about the target. Therefore, if the relative orbits do not have any intersection, collisions are impossible.



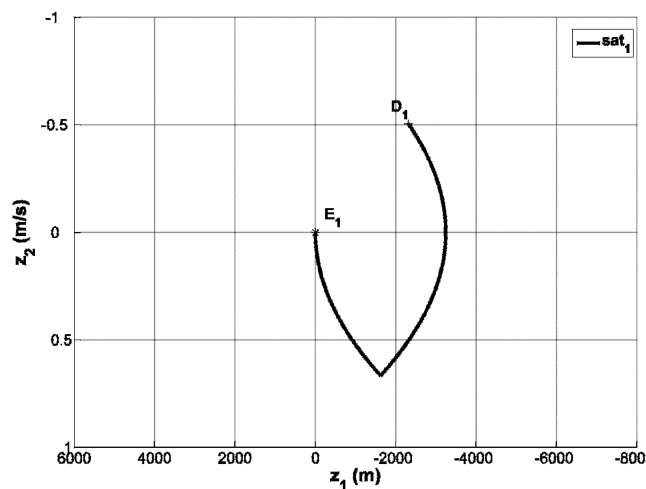
a) First sequence: Sat₄ is stabilized



b) Second sequence: Sat₃ is stabilized



c) Third sequence: Sat₂ is stabilized



d) Fourth sequence: Sat₁ is stabilized

Fig. 5 Simulation results: phase 1, relative orbit stabilization, spacecraft trajectories in the z_1 - z_2 plane.

3. Collision Avoidance

Potential collisions are possible during all of the phases of the maneuver and need to be taken into account. Because the control calculation is completely analytical, the full maneuver sequence can be recomputed with a small computational burden. Therefore, the following simple strategy is adopted for collision avoidance: the whole maneuver sequence is precomputed and, if any collisions are foreseen, an initial coasting time is iteratively introduced for the whole fleet until all collisions are avoided.

IV. Simulation Results

This section reports the simulation results for the sample case of a fleet of five homogenous spacecraft (1 target and 4 chasers). The proposed control policy is applied first by considering the linear dynamics model. To further validate the reliability and robustness of the proposed method, an application of the algorithm to a non-Keplerian orbital propagator is also presented.

A. Linear Dynamics Simulation (5 Spacecraft)

Table 1 reports the chosen values for the main characteristics of the spacecraft, Table 2 reports the values of the initial conditions, and Table 3 reports the values of additional simulation parameters.

The maximum value of drag for any spacecraft of the fleet (drag plate opened orthogonally to the velocity direction) corresponding to the parameter values listed in Table 1 is

$$u_y = 4.55 \times 10^{-5} \text{ m} \cdot \text{s}^{-2} \quad (17)$$

Figures 5–11 report the simulation’s results corresponding to the value of parameters listed in Tables 1–3. The control sequence was determined according to the algorithms described in Sec. III. In particular, Fig. 5 reports the trajectories of the spacecraft in the z_1 – z_2 plane during the stabilization phase of the maneuver. The control algorithm first drives the chaser spacecraft (designated as Sat₄) into a stable orbit about the target (see Fig. 5a), then Sat₃ (see Fig. 5b), Sat₂ (see Fig. 5c), and Sat₁ (see Fig. 5d), respectively. In the plots, crosses indicate initial states and stars indicate final states (either referred to a single sequence or the overall stabilization phase). Portions of the maneuver during which some of the spacecraft drift away can be recognized as straight lines parallel to the z_1 axis. Drifting phases arise, according to the algorithm introduced in Sec. III, when a spacecraft has to wait for the others that need to maneuver first due to their higher relative energy [Eq. (16)]. Collisions did not occur during this simulation; that is, no collision-avoidance strategy was required.

Figure 6 reports the evolution of the states z_3 and z_4 during the stabilization phase of the maneuver. Figure 7 presents the time history of the differential drag control acting on each of the four chaser spacecraft during the four sequences of the stabilization maneuver corresponding to Fig. 5. Positive drag indicates that a chaser is opening the drag plate but the target is not, negative drag indicates the target opening its drag plate but the chaser is not, and zero drag corresponds to one of the two following cases: a) both target and chaser are opening their plates and b) both target and

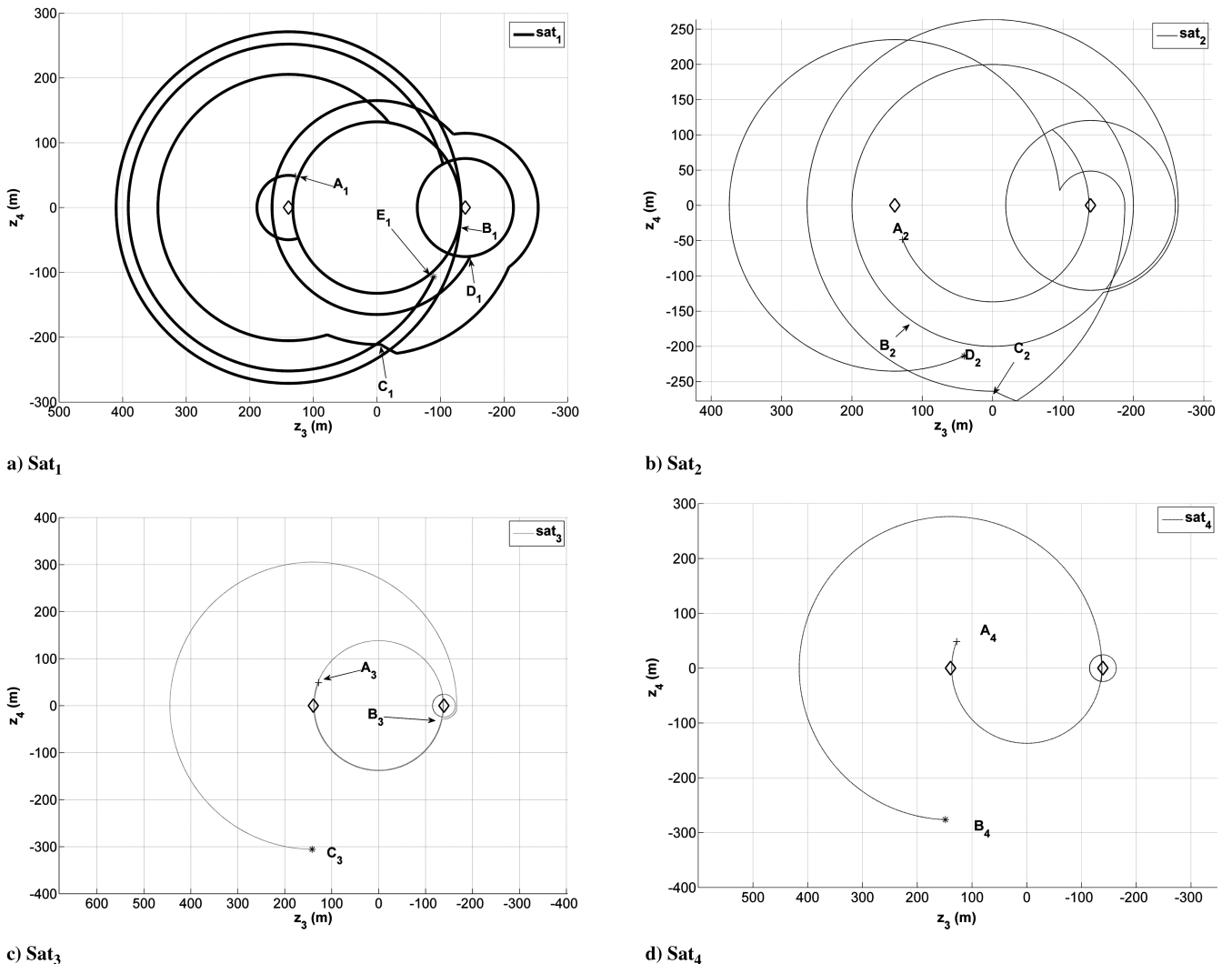


Fig. 6 Simulation results: phase 1, relative orbit stabilization, spacecraft trajectories in the z_3 – z_4 plane.

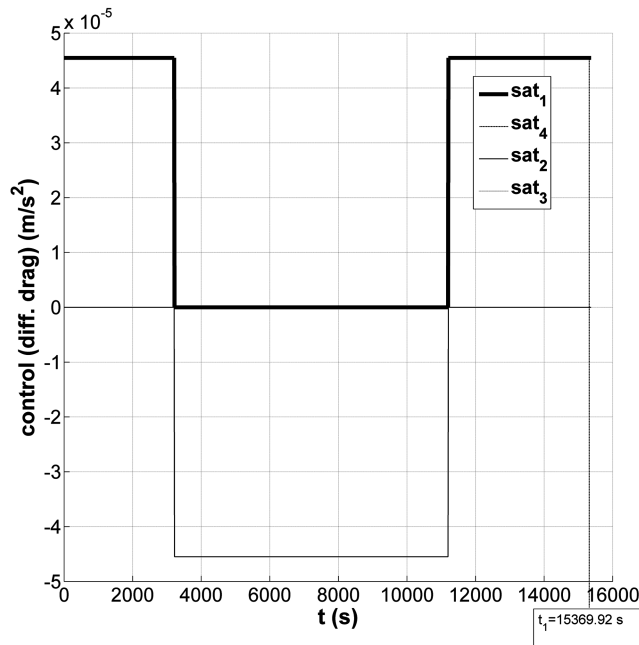
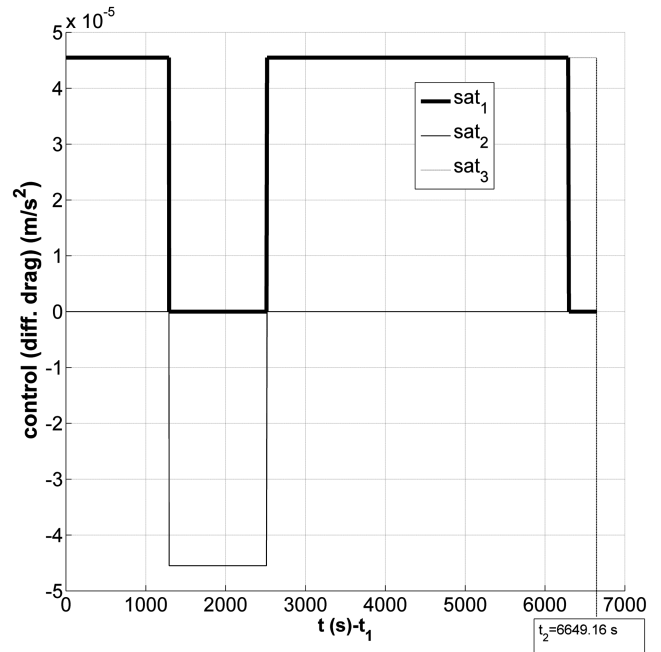
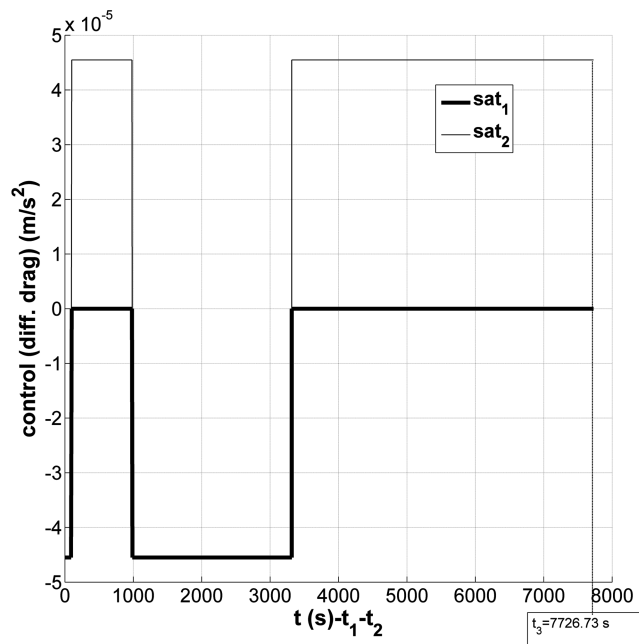
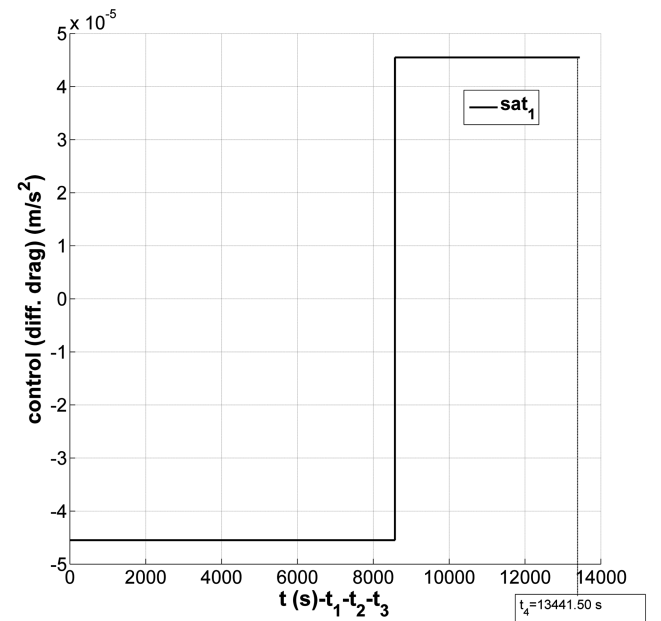
a) First sequence: Sat₄ is stabilizedb) Second sequence: Sat₃ is stabilizedc) Third sequence: Sat₂ is stabilizedd) Fourth sequence: Sat₁ is stabilized

Fig. 7 Simulation results: phase 1, relative orbit stabilization, differential drag acting on each chaser spacecraft with respect to the target during the four sequences corresponding to Fig. 5.

chaser are keeping their plates closed. The control sequences in Fig. 7 can be realistically implemented. In particular, any chattering behavior is absent. Figure 8 shows the trajectories in the Δx - Δy plane during the spacecraft stabilization phase.

The required time for the stabilization phase of the maneuver was 12.04 h (7.89 orbital periods). The residual distances of the chaser spacecraft from the target at the end of the stabilization phase are reported in Table 4.

After the stabilization phase, the final rendezvous is achieved by applying sequentially, to each of the chaser spacecraft, the algorithm introduced in Sec. III.A.2, by starting from the closest one. In particular, Fig. 9 reports the trajectory Sat₃, which is the one ending its stabilization phase the furthest from the target. The applied control sequence leads Sat₃ to the rendezvous condition. The approach introduced in Sec. III.A.2 can be easily recognized: the uncontrolled

waiting phase is followed first by a positive control phase for which the duration is Δt^* [see Eq. (14)], then by a negative control phase of duration $2\Delta t^*$, and, finally, by a positive control phase of duration Δt^* . The effect in the z_1 - z_2 plane is that of generating a closed symmetric trajectory (see Fig. 10), as was expected. Figure 11 shows the trajectory in the Δx - Δy plane. The rendezvous of the other three chasers with respect to the target follow an analogous sequence of events; therefore, the detailed results are omitted for the sake of brevity.

The rendezvous phase of the maneuver for Sat₃ takes 1.67 h to complete (1.1 orbital periods). The completion of the rendezvous phase of the maneuver for the whole fleet takes 6.16 h (4.037 orbital periods). Finally, the entire maneuver, bringing the chaser spacecraft from their generic initial conditions to the rendezvous with the target, takes 18.16 h (11.90 orbital periods).

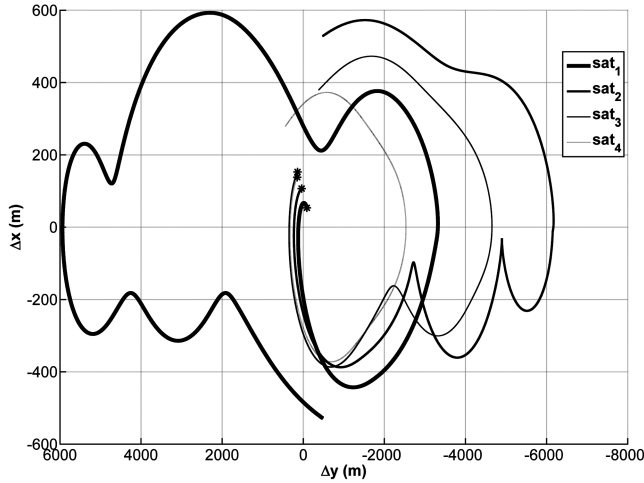


Fig. 8 Simulation results: phase 1, relative orbit stabilization, spacecraft trajectories in the Δx - Δy plane. Stars indicate the beginning of the stable orbiting condition of each chaser about the target.

For comparison purposes, the Leonard et al.'s [5,6] approach applied to Sat₃ with the same initial conditions at the end of the stabilization phase results in a final condition with a residual distance of 47.45 m from the target and a maneuver time of 18.09 h (for the rendezvous phase only).

To estimate the validity of the constant-air-density approximation assumed in our development, an approximate calculation for the orbit decay was performed through Eq. (18), resulting in the following variation of the semimajor axis for one orbit:

$$\Delta a_{\text{orb}}(T) = -2\pi(C_D S/m)\rho a_{\text{orb}}^2 \quad (18)$$

Applying Eq. (18) to our 350 km orbit case gives $\Delta a_{\text{orb}} = -0.44$ km. By considering this decay constant as a worst-case scenario (i.e., every spacecraft has the drag plate constantly open), the altitude decay is ~ 5.3 km during the 18.16 h of the maneuver. Therefore, the increase in atmospheric density appears to be negligible.

In this section, the results are reported for a set of Monte Carlo simulations performed to validate the robustness of the control algorithm introduced in Sec. III. In particular, a normal distribution of relative positions and velocities has been generated with the following boundaries, and 1000 simulation runs have been performed:

$$\begin{aligned} -3.2 \text{ km} < \Delta x < 3.2 \text{ km} & \quad -3.2 \text{ km} < \Delta y < 3.2 \text{ km} \\ -0.1144 \text{ m/s} < \Delta \dot{x} < 0.1144 \text{ m/s} & \\ -5.54 \text{ m/s} < \Delta \dot{y} < 5.54 \text{ m/s} & \end{aligned} \quad (19)$$

The first result of the Monte Carlo analysis consists of the confirmation of the robustness of the stabilization algorithm. In particular, during all of the simulation runs, all of the chasers were stabilized with respect to the target. The second result of the Monte Carlo analysis consists of the confirmation of the collision-avoidance capability of the proposed control algorithm. In particular, in 20 of the 1000 simulation cases, the collisions were successfully

Table 4 Stabilization maneuvers final distances

Sat ₁	103.97 m
Sat ₂	142.72 m
Sat ₃	329.77 m
Sat ₄	157.81 m

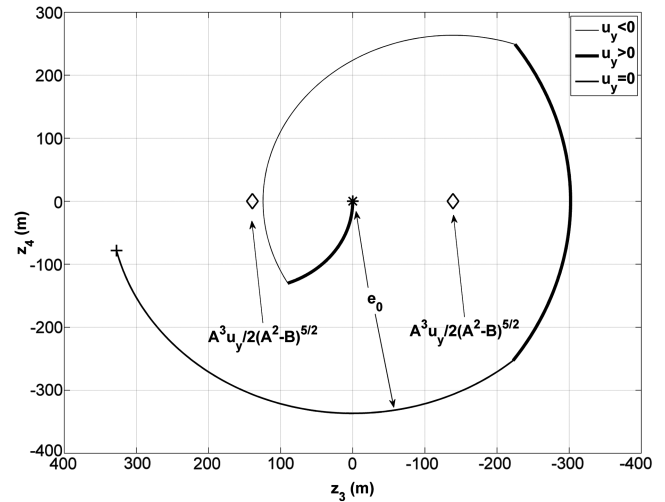


Fig. 9 Simulation results: phase 2, rendezvous with the target, trajectory of Sat₃ in the z_3 - z_4 plane. The + indicates the initial state, and the * indicates the final condition.

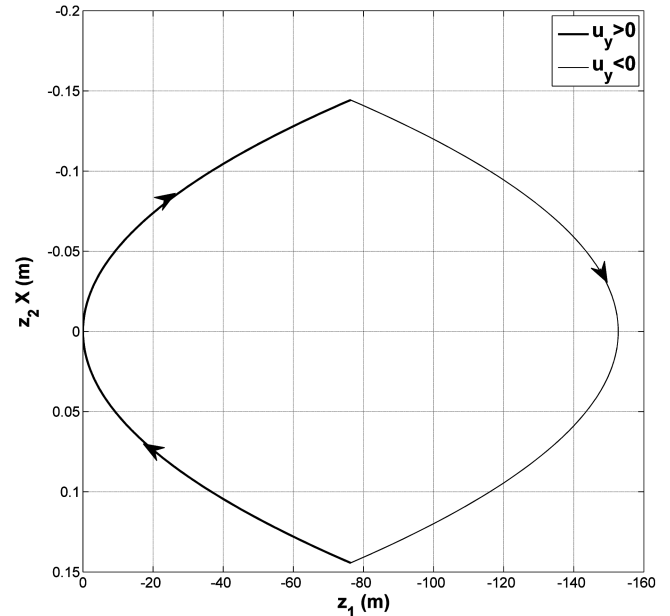


Fig. 10 Simulation results: phase 2, rendezvous with the target, trajectory of Sat₃ in the z_1 - z_2 plane.

avoided by adding an initial coasting phase, according to the algorithm introduced in Sec. III.B.3. In all of the other cases, no collisions were occurring.

The third result of the Monte Carlo analysis consists of the confirmation of the reasonable maneuvering time. In particular, Fig. 12 reports the required maneuver time as a function of the initial mean distance of the chasers from the target. Figure 12 reflects an intuitively expected behavior: the total time to stabilize the whole fleet increases with the mean distance of the spacecraft from the target.

Finally, it is worth noting that maneuvers of longest duration (see Fig. 12), lasting about 150 h, required less than 2 min to be completely generated on a Pentium D 3.2 Ghz machine (corresponding to $\sim 0.02\%$ of the maneuver duration).

B. Nonlinear Dynamics Simulation

In this simulation, one chaser spacecraft has to rendezvous with a target that has orbital parameters similar to those of the International

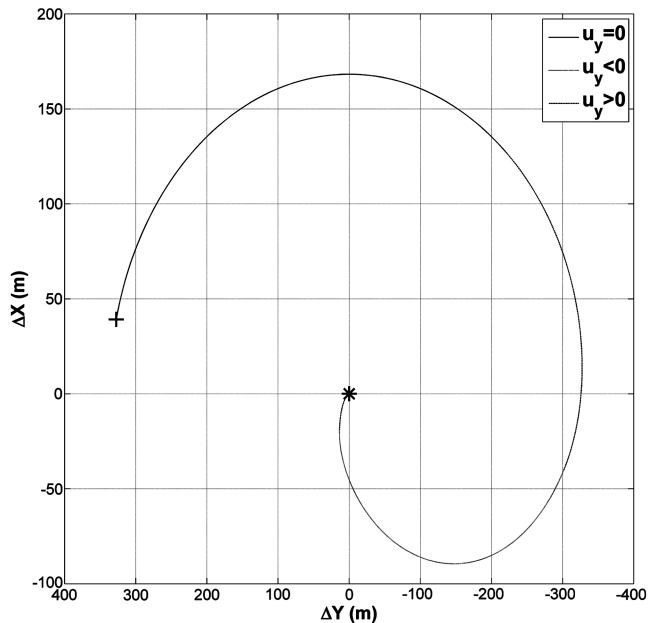


Fig. 11 Simulation results: phase 2, rendezvous with the target, trajectory of Sat₃ in the Δx - Δy plane. The + indicates the initial state, and the * indicates the final condition.

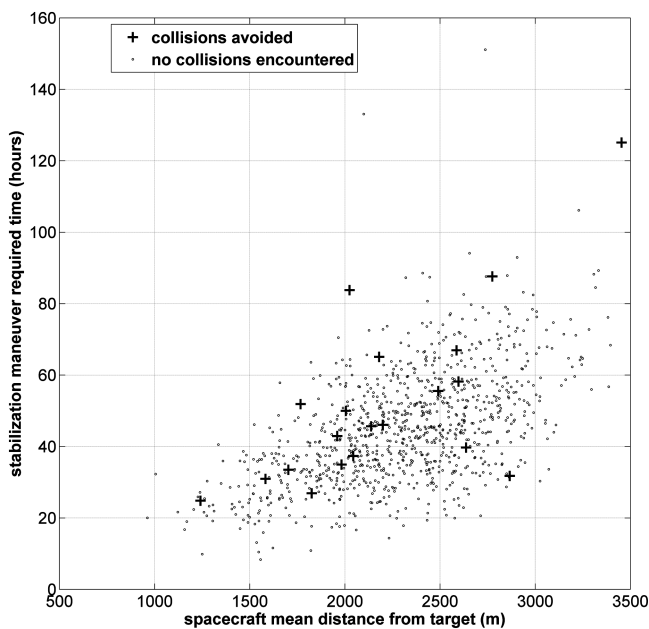


Fig. 12 Monte Carlo analysis required time for completing the maneuver.

Space Station. The motion of the chaser and the target spacecraft are separately obtained by using a non-Keplerian orbital propagator. Then their relative state vector is computed and projected in the local-vertical/local-horizontal (LVLH) frame, centered at any time on the

Table 5 Orbital parameters of the target and chaser for complete dynamics case

Target spacecraft	Chaser spacecraft
$a_{ISS} = 6713889.83$ m	$a_{ISS} = 6713889.83$ m
$e_{ISS} = 0$	$e_{ISS} = 0$
$i_{ISS} = 51.94116$ deg	$i_{ISS} = 51.94116$ deg
$\Omega_{ISS} = 206.35768$ deg	$\Omega_{ISS} = 206.35768$ deg
$\omega_{ISS} = 101.07112$ deg	$\omega_{ISS} = 101.07112$ deg
$\nu_{ISS} = 108.08480$ deg	$\nu_{ISS} = 108.08480 + 0.03$ deg

Table 6 Spacecraft characteristics and reference atmospheric density

Mass, kg	10
Maximum deployable area, m ²	1
Minimum crosswind area (plates closed), m ²	.25
C_D	2.2
$\rho_{336 \text{ km}}, \text{ kg} \cdot \text{m}^{-3}$	1.3×10^{-11} [16]

target spacecraft. The relative orbit feedback stabilization control is used to drive the opening and closing of the drag plates. During the second phase of the rendezvous maneuver, the analytical algorithm presented in Sec. III.B is applied as a feedforward control. The controller is based on the linear dynamics and it still assumes a constant value of atmospheric density, as in the previous simulations (Sec. IV.A)

The orbital propagation for chaser and target takes into account the following effects [16]: 1) Earth's gravitational field harmonics up to J_4 , 2) variable density on both target and chaser, 3) moon-sun third-body effects, and 4) solar radiation pressure.

Table 5 reports the two spacecraft orbital elements at initial time, corresponding to the following relative state in the LVLH coordinate system:

$$\begin{bmatrix} x \\ y \\ \dot{x} \\ \dot{y} \end{bmatrix} = \begin{bmatrix} -156.4 \text{ m} \\ 3515.3 \text{ m} \\ -0.5 \text{ m/s} \\ 0.4 \text{ m/s} \end{bmatrix} \quad (20)$$

The initial altitude of the spacecraft is approximately 336 km. The reference atmospheric density value for such altitude is reported in Table 6, together with additional characteristics of the spacecraft. The constant reference value for the atmospheric density is used within the controller. The spacecraft are assumed to be cubes with a 0.5 m side.

Figure 13 shows the rendezvous trajectory when the linear-dynamics-based controller is applied to the complete dynamics. The whole maneuver takes approximately 6 h to complete. The same figure also shows when the feedforward controller takes over, after the relative orbit stabilization, and the final rendezvous error position, due to disturbances, nonlinear dynamics, and nonconstant density.

Both the chaser and the target present an orbit decay of about 4 km after the maneuver is complete. The results shown in Fig. 13 indicate that the proposed control policy is robust with respect to disturbances and higher-order orbital effects.

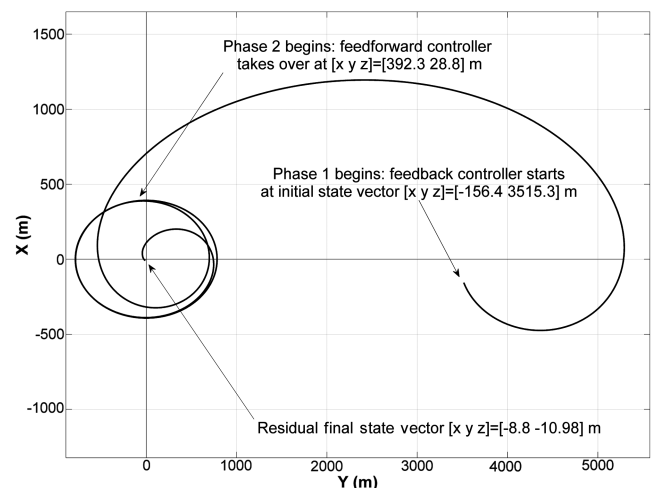


Fig. 13 Rendezvous trajectory for the complete dynamics case.

V. Conclusions

New control logic has been introduced for the relative orbit stabilization and the subsequent rendezvous of multiple spacecraft by exploiting the differential atmospheric drag. By varying the level of aerodynamic drag of each spacecraft, relative differential accelerations are generated among the spacecraft of the group and therefore their relative orbits are controlled. The proposed method can be used, for instance, for an on-orbit assembly mission.

The recently developed Schweighart–Sedwick model was used to describe the relative dynamics of different spacecraft nearby a circular orbit with the inclusion of the J_2 effects. Furthermore, the natural relative dynamics of each chaser with respect to the target is decoupled into a secular motion and a periodic oscillation. In particular, the following two-phase control method was proposed. First, the secular motion of each chaser is controlled via differential drag for the spacecraft to sequentially move from an arbitrary initial condition to a closed stable relative orbit around the target spacecraft. After the relative orbit stabilization, a relative eccentricity control is applied to each spacecraft to zero-out the semi-axis of the relative orbit around the target and achieve the rendezvous condition.

Collisions are avoided by introducing a coasting phase before the control takes action and recomputing the whole trajectory. This is possible thanks to the analytical nature of the proposed solution, which allows for an easy and computationally light recalculation of the whole maneuvering history.

A sample simulation was conducted by considering five spacecraft. The robustness of the stabilization control logic, collision-avoidance capability, and the reasonable amount of time required for the maneuver were validated through Monte Carlo analysis. To establish the robustness of the control logic here proposed, a two-spacecraft rendezvous simulation was performed using a non-Keplerian orbital propagator. The drag control was used in a feedback fashion for the stabilization phase and as a feedforward for the rendezvous phase. A limitation of the proposed control approach is that the final rendezvous orbit cannot be a priori specified.

The proposed methodology is applicable to a generic number of spacecraft with on–off air drag device capabilities. The possibility of using the proposed passive orbital control for low-Earth-orbit spacecraft is attractive because it allows for long-term propellant-free formation maneuvering.

Acknowledgments

This research was partially supported by the Defense Advanced Research Projects Agency. This research was performed while R. Bevilacqua was holding a National Research Council Research Associateship Award at the Spacecraft Robotics Laboratory of the Naval Postgraduate School. The authors wish to thank Lt. Cmdr.

Jason Hall for the useful discussions and for the fundamental help regarding the control integration into a complete orbital propagator.

References

- [1] Palmerini, G. B., Sgubini, S., and Taini, G., “Spacecraft Orbit Control Using Air Drag,” International Astronautical Congress Paper 05-C1.6.10, 2005.
- [2] Humi, M., and Carter, T., “Motions in a Central Force Field with a Quadratic Model,” American Astronautical Society Paper 03-238, 2003, pp. 2005–2018.
- [3] Carter, T., and Humi, M., “Clohessy-Wiltshire Equations Modified to Include Quadratic Drag,” *Journal of Guidance, Control, and Dynamics*, Vol. 25, No. 6, Nov.–Dec. 2002, pp. 1058–1063.
- [4] Humi, M., and Carter, T., “Fuel-Optimal Rendezvous in a Central Force Field with Linear Drag,” American Astronautical Society Paper 01-236, 2001, pp. 1875–1892.
- [5] Leonard, C. L., Hollister, W. M., and Bergmann, E. V., “Orbital Formationkeeping with Differential Drag,” *Journal of Guidance, Control, and Dynamics*, Vol. 12, No. 1, 1989, pp. 108–113. doi:10.2514/3.20374
- [6] Leonard, C. L., “Formationkeeping of Spacecraft Via Differential Drag,” M.Sc. Thesis, Massachusetts Inst. of Technology, Cambridge, MA, July 1986.
- [7] Campbell, M. E., “Planning Algorithm for Multiple Satellite Clusters,” *Journal of Guidance, Control, and Dynamics*, Vol. 26, No. 5, 2003, pp. 770–780.
- [8] Guelman, M., and Aleshin, M., “Optimal Bounded Low-Thrust Rendezvous with Fixed Terminal-Approach Direction,” *Journal of Guidance, Control, and Dynamics*, Vol. 24, No. 2, 2001, pp. 378–385.
- [9] Bevilacqua, R., and Romano, M., “Optimal Guidance of Proximity Maneuvers for a Spacecraft with Hybrid On-Off Continuous and Impulsive Thrust,” *Journal of Guidance, Control, and Dynamics*, Vol. 30, No. 4, 2007, pp. 1175–1178. doi:10.2514/1.27716
- [10] Clohessy, W. H., and Wiltshire, R. S., “Terminal Guidance System for Satellite Rendezvous,” *Journal of the Aerospace Sciences*, Vol. 27, No. 9, 1960, pp. 653–658.
- [11] Schweighart, S. A., and Sedwick, R. J., “High-Fidelity Linearized J_2 Model for Satellite Formation Flight,” *Journal of Guidance, Control, and Dynamics*, Vol. 25, No. 6, 2002, pp. 1073–1080.
- [12] Kumar, K. D., Bang, H. C., and Tahk, M. J., “Satellite Formation Flying Using Along-Track Thrust,” *Acta Astronautica*, Vol. 61, Nos. 7–8, Oct. 2007, pp. 553–564. doi:10.1016/j.actaastro.2007.01.069
- [13] Starin, R. S., Yedavalli, R. K., and Sparks, A. G., “Spacecraft Formation Flying Maneuvers Using Linear-Quadratic Regulation with No Radial Axis Input,” AIAA Guidance, Navigation, and Control Conference and Exhibit, Montreal, AIAA Paper 2001-4029, Aug. 2001.
- [14] Bevilacqua, R., Romano, M., and Curti, F., “Decoupled-Natural-Dynamics for the Relative Motion of Two Spacecraft Without and with J_2 Perturbation,” *Journal of Guidance, Control, and Dynamics* (submitted for publication).
- [15] Pontryagin, L. S., Boltjanskiy, V. G., Gamkrelidze, R. V., and Mishenko, E. F., *The Mathematical Theory of Optimal Processes*, Wiley-Interscience, New York, 1969, pp. 27–35.
- [16] Wertz, J. R., and Larson, W. J., *Space Mission Analysis and Design*, 3rd ed., Space Technology Series, Microcosm Press, El Segundo, CA, 1999.